Redox Properties of $C_6S_8^{n-}$ and $C_3S_5^{n-}$ ($n = 0, 1, 2$): Stable Radicals and Unusual Structural Properties for C−S−S−C Bonds

Jonathan G. Breitzer, Alex I. Smirnov,† Lisa F. Szczepura,‡ Scott R. Wilson, and Thomas B. Rauchfuss*

School of Chemical Sciences and the Frederick Seitz Materials Research Laboratory, University of Illinois at Urbana−Champaign, Urbana, Illinois 61801

Received September 5, 2000

The new anionic carbon sulfides $C_6S_{10}^{2-}$ and $C_{12}S_{16}^{2-}$ are described and crystallographically characterized. The $C_{12}S_{16}^{2-}$ anion consists of two C_6S_8 units connected by an exceptionally long (2.157(12) Å) S−S bond. In solution, $C_{12}S_{16}^{2-}$ exists in equilibrium with the radical $C_6S_8^{-\bullet}$. The equilibrium constant for radical formation (293 K, THF) is 1.2×10^{-4} M, as determined by optical spectroscopy at varying concentrations. Radical formation occurs through scission of the S−S bond. On the basis of variable temperature EPR spectra, the thermodynamic parameters of this process are $\Delta H = +51.5 \pm 0.5$ kJ mol^{-1} and $\Delta S = +110 \pm 3$ J mol^{-1} K^{-1}. $C_6S_{10}^{2-}$ is an oxidation product of $C_3S_5^{2-}$ and consists of two C_3S_5 units connected by an S−S bond. The S−S bond length (2.135(4) Å) is long, and the CS−SC torsion angle is unusually acute (52.1°), which is attributed to an attractive interaction between C_3S_2 rings. The oxidation of $(Me_4N)_2C_3S_5$ occurs at −0.90 V vs Fc^+/Fc in MeCN, being further oxidized at −0.22 V. The similarity of the cyclic voltammogram of $(Me_4N)_2C_6S_{10}$ to that of $(Me_4N)_2C_3S_5$ indicates that $C_6S_{10}^{2-}$ is the initial oxidation product of $C_3S_5^{2-}$.

Introduction

Carbon sulfides represent a stoichiometrically simple but structurally complex family of molecules and solids consisting of thermodynamically robust C═C, C−S, and S−S bonds.[1] For this reason, the carbon sulfides are a promising source of inexpensive new materials for photonics,[2] electrical conductors,[3] charge storage materials (secondary batteries),[4] and catalyst supports. The aspect of particular interest in these materials is the presence of S−S bonds, which are amenable to cleavage without alteration of the C−C, C−S, and C═S linkages. In recent years, several new binary carbon sulfide polymers and molecules have been described.[5] In addition to the binary carbon sulfides, numerous anionic carbon sulfides are also known, some of which are key precursors in the area of molecular electronics.[6]

Carbon sulfides and their anionic analogues generally follow the octet rule. An exception is C_9S_9, which features three T-shaped hypervalent sulfur atoms.[7] Another possible exception is the even-electron species $[C_8S_8^{2-}]_n$,[8] which is paramagnetic in solution. The synthesis of nonoctet carbon sulfide species should be attainable through one-electron reduction of carbon sulfides with S−S bonds. The one-electron reduction of S−S bonds to make disulfide radical anions has precedence in the literature: thiyl radicals ($RS^\bullet$) have been implicated as a complicating factor in the kinetics of the oxidation of the positive electrode (recharging process) of lithium organodisulfide storage batteries.[9] Generally, however, thiyl radicals and disulfide radical anions are unstable.

Both families of molecules under study in this paper, $C_6S_8^{n-}$ and $[C_3S_5]_m^{n-}$, are derived from $C_3S_5^{2-}$, also called $dmit^{2-}$. $C_3S_5^{2-}$ is the central intermediate in carbon sulfide chemistry because of its efficient synthesis from CS_2 and the utility of its derivatives in materials science.[10] C_6S_8 is prepared by the addition of HCl to $[Zn(C_3S_5)_2]^{2-}$ to give $C_3S_5H_2$, which eliminates H_2S.[11] We have previously shown that C_6S_8 can be reduced using excess $LiBHEt_3$ to give the dianion $C_6S_8^{2-}$,[12] the

† Present address: Department of Chemistry, North Carolina State University, Raleigh, NC 27695-8204.

‡ Present address: Department of Chemistry, Illinois State University, Normal, IL 61790-4160.

(1) Doxsee, D. D.; Galloway, C. P.; Rauchfuss, T. B.; Wilson, S. R.; Yang, X. *Inorg. Chem.* **1993**, *32*, 5467.
(2) Breitzer, J. G.; Dlott, D. D.; Iwaki, L. K.; Kirkpatrick, S. M.; Rauchfuss, T. B. *J. Phys. Chem.* **1999**, *103*, 6930.
(3) Pullen, A. E.; Abboud, K. A.; Reynolds, J. R.; Piotraschke, J.; Zeltner, S.; Olk, R. M.; Hoyer, E.; Liu, H. L.; Tanner, D. B. *Synth. Met.* **1997**, *86*, 1791.
(4) (a) Naoi, K.; Kawase, K.-i.; Inoue, Y. *J. Electrochem. Soc.* **1997**, *144*, L170. (b) Picart, S.; Geniès, E. *J. Electroanal. Chem.* **1996**, *408*, 53. (c) Doeff, M. M.; Lerner, M. M.; Visco, S. J.; Jonghe, L. C. D. *J. Electrochem. Soc.* **1992**, *139*, 2077. (d) Liu, M.; Visco, S. J.; Jonghe, L. C. D. *J. Electrochem. Soc.* **1989**, *136*, 2570.
(5) (a) Cataldo, F. *Inorg. Chim. Acta* **1995**, *232*, 27. (b) Yang, X.; Rauchfuss, T. B.; Wilson, S. R. *J. Am. Chem. Soc.* **1989**, *111*, 3465. (c) Richter, A. M.; Fanghänel. E. *Tetrahedron Lett.* **1983**, *24*, 3577. (d) Lu, F. L.; Keshavarz, K. M.; Srdanov, G.; Jacobson, R. H.; Wudl, F. *J. Org. Chem.* **1989**, *54*, 2165. (e) Schumaker, R. R.; Engler, E. M. *J. Am. Chem. Soc.* **1977**, *99*, 5521.
(6) Cassoux, P.; Valade, L.; Kobayashi, H.; Kobayashi, A.; Clark, R. A.; Underhill, A. E. *Coord. Chem. Rev.* **1991**, *110*, 115.
(7) (a) Brown, J. P.; Gay, T. B. *J. Chem. Soc., Perkin Trans. 1* **1974**, 866. (b) Hansen, L. K.; Hordvik, A. *J. Chem. Soc., Chem. Commun.* **1974**, 800.
(8) Chou, J.-H.; Rauchfuss, T. B. *J. Am. Chem. Soc.* **1997**, *119*, 4537.
(9) Liu, M.; Visco, S. J.; Jonghe, L. C. D. *J. Electrochem. Soc.* **1990**, *137*, 750.
(10) Pullen, A. E.; Abboud, K. A.; Reynolds, J. R.; Piotraschke, J.; Zeltner, S.; Olk, R. M.; Hoyer, E.; Liu, H. L.; Tanner, D. B. *Synth. Met.* **1997**, *86*, 1791.
(11) Galloway, C. P.; Doxsee, D. D.; Fenske, D.; Rauchfuss, T. B.; Wilson, S. R.; Yang, X. *Inorg. Chem.* **1994**, *33*, 4537.
(12) Chou, J.-H.; Rauchfuss, T. B.; Szczepura, L. F. *J. Am. Chem. Soc.* **1998**, *120*, 1805.

10.1021/ic000999r CCC: $20.00
Published on Web 03/02/2001

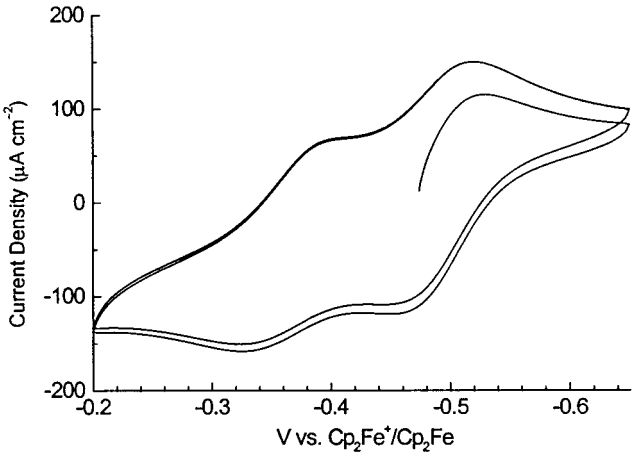

Figure 1. Cyclic voltammogram of $(Ph_4P)_2(C_{12}S_{16})$, 1×10^{-3} M in acetonitrile: electrolyte, 0.1 M Bu_4NPF_6; working electrode, glassy carbon; scan rate, 0.1 V/s. Potentials are referenced to Fc^+/Fc.

electrochemistry of which revealed the presence of an intermediate oxidation state:

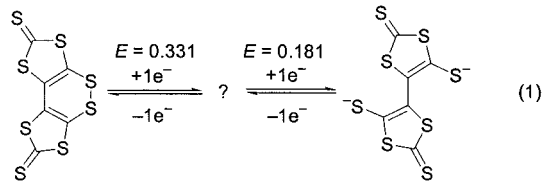

(potentials referenced to NHE). In this paper, we characterize this intermediate oxidation state.

Species with the formula $[C_3S_5]_n$ are formed upon oxidation of $[Zn(C_3S_5)_2]^{2-}$ by SO_2Cl_2.[13] $[C_3S_5]_n$ exists in two forms: a dimer (C_6S_{10}), which is slightly soluble in CS_2 and has been crystallographically characterized, and an insoluble polymer. In conjunction with our study of the oxidation states of $(C_6S_8)^{n-}$, we investigated the intermediate oxidation states between $C_3S_5^{2-}$ and C_6S_{10}. Whereas the coordination[3,14] and organic[15] chemistry of $C_3S_5^{2-}$ is vast, almost nothing is known of the fundamental redox properties of this anion. We have recently described the optical properties of $C_3S_5^{2-}$.[16]

Results

Synthesis of the Radical $C_6S_8^{-\bullet}$. The cyclic voltammogram of $C_6S_8^{2-}$ (Figure 1) consists of two features corresponding to successive one-electron oxidations of the dianion to give the neutral C_6S_8. The $\Delta E_{1/2}$ for the two redox couples is 142 mV. This difference reflects the stability of the intermediate species $C_6S_8^{-\bullet}$ with respect to disproportionation. The disproportionation constant, K_{disp}, is the inverse of the comproportionation constant, K_{com}, which is defined in

$$C_6S_8 + C_6S_8^{2-} \rightleftharpoons 2C_6S_8^{-\bullet} \qquad (2)$$

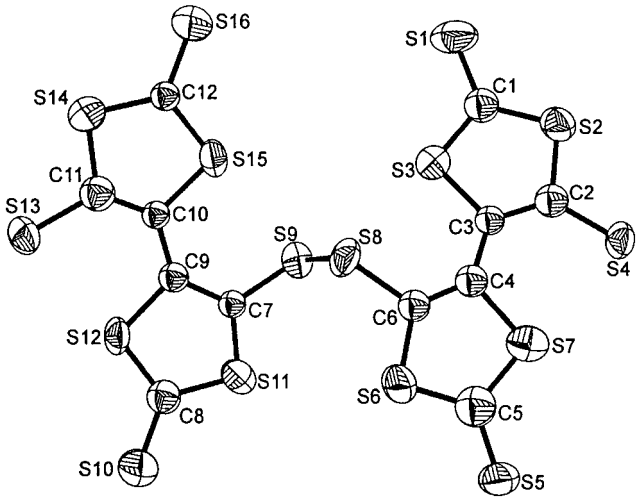

Figure 2. Molecular structure of the anion in $(Ph_4P)_2(C_{12}S_{16})$ with thermal ellipsoids drawn at the 50% probability level.

By use of the equation $\ln K_{com} = RT/[nF(\Delta E_{1/2})]$ $(=K_{disp}^{-1})$, K_{com} was calculated to be 214. This value of K_{com}, being much greater than 1, indicates that $C_6S_8^{-\bullet}$ should be stable and that solutions thereof should be relatively free of C_6S_8 and $C_6S_8^{2-}$. The value of K_{com} does not indicate the degree of aggregation of $C_6S_8^{-\bullet}$.

The mildness and reversibility of the redox properties of C_6S_8 encouraged us to pursue the isolation of the intermediate species $C_6S_8^{-\bullet}$. The comproportionative synthesis was effected by combining a solution of $(Ph_4P)_2C_6S_8$ with C_6S_8:

$$C_6S_8 + C_6S_8^{2-} \rightleftharpoons 2C_6S_8^{-\bullet} \rightleftharpoons C_{12}S_{16}^{2-} \qquad (3)$$

A solution of $C_6S_8^{2-}$, which is purplish-red, became deep-brown upon addition of an equimolar amount of C_6S_8 (which is insoluble). After several hours, the brown solution was filtered; dilution of the filtrate with ether gave $(Ph_4P)(C_6S_8)$. Samples of this compound are moderately stable in air and can be obtained in analytical purity. Solutions in THF are also stable for a few days in the absence of air. Subsequent experiments (see next section) established that $C_6S_8^{-\bullet}$ exists in equilibrium with the dimer $C_{12}S_{16}^{2-}$ (see eq 3).

Single crystals of the nominal 1:1 salt $(Ph_4P)(C_6S_8)$ were obtained from THF/hexanes solutions. The reflection data were weak, but a sensible solution was achieved that confirmed the connectivity expected for the dimer $C_{12}S_{16}^{2-}$ (Figure 2). The dianion consists of a pair of $C_6S_8^{-\bullet}$ moieties connected by an S−S bond. Although it would appear that the dianion itself should have a C_2 axis through the S−S bond, there are no crystallographically imposed symmetry elements in the $C_{12}S_{16}^{2-}$ unit.

The C_6S_8 subunits in $C_{12}S_{16}^{2-}$ are unremarkable and compare closely to the dianion of $(Ph_4P)_2(C_6S_8)$.[12] The S−S bond length, though, is 2.154 Å, and the associated CS−SC torsion angle (dihedral angle) is 108.5°. This geometry is unusual for organic disulfides (see Discussion). Selected angles and distances for the anion in $(Ph_4P)_2(C_{12}S_{16})$ are listed in Table 1.

Optical Properties of the Radical $C_6S_8^{-\bullet}$. Concentrated THF solutions of $(PPh_4)(C_6S_8)$ are deep-brown, whereas dilute solutions are brilliant violet. Because $C_6S_8^{-\bullet}$ is an odd-electron species and in view of the structure of $C_{12}S_{16}^{2-}$, we propose an

(13) Yang, X.; Rauchfuss, T. B.; Wilson, S. *J. Chem. Soc., Chem. Commun.* **1990**, 34. Neilands, O.; Kacens, J.; Kreicberga, J. *Zh. Org. Khim.* **1989**, *25*, 658.

(14) (a) Canadell, E. *Coord. Chem. Rev.* **1999**, *185*, 629. (b) Cassoux, P. *Coord. Chem. Rev.* **1999**, *185*, 213. (c) Underhill, A. E.; Clark, R. A.; Clemenson, P. I.; Friend, R.; Allen, M.; Marsden, I.; Kobayashi, A.; Kobayashi, H. *Phosphorus, Sulfur Silicon Relat. Elem.* **1992**, *67*, 311. (d) Olk, R.-M.; Olk, B.; Dietzsch, W.; Kirmse, R.; Hoyer, E. *Coord. Chem. Rev.* **1992**, *117*, 99. (e) Cassoux, P.; Valade, L.; Kobayashi, H.; Kobayashi, A.; Clark, R. A.; Underhill, A. E. *Coord. Chem. Rev.* **1991**, *110*, 115.

(15) Svenstrup, N.; Becher, J. *Synthesis* **1995**, 215.

(16) Breitzer, J. G.; Rauchfuss, T. B. *Polyhedron* **2000**, *19*, 1283.

Table 1. Selected Angles (deg) and Distances (Å) for the Anion in $(Ph_4P)_2(C_{12}S_{16})$

S(8)−S(9)	2.157(12)	S(9)−C(7)	1.79(2)
S(8)−C(6)	1.82(3)	S(6)−C(6)	1.68(3)
C(4)−C(6)	1.35(3)	S(7)−C(4)	1.79(3)
C(3)−C(4)	1.42(3)	C(6)−S(8)−S(9)	104.4(9)
C(2)−C(3)	1.41(3)	C(6)−C(4)−C(3)	131.6(27)
S(4)−C(2)	1.69(3)	C(6)−S(8)−S(9)−C(7)	108.5

equilibrium between $C_6S_8^{-\bullet}$ radicals and $C_{12}S_{16}^{2-}$ dimers to explain the concentration-dependent optical properties, where the violet $C_6S_8^{-\bullet}$ becomes relatively more predominant at lower concentrations.

We examined the concentration-dependent optical properties of $C_6S_8^{-\bullet}$ using electronic spectroscopy. THF solutions (3.3×10^{-6} M $< C_{C_{12}S_{16}^{2-}} < 6.5 \times 10^{-4}$ M) were prepared, where $C_{C_{12}S_{16}^{2-}}$ represents the analytical concentration of the dimer; i.e., the amount of $(Ph_4P)_2(C_{12}S_{16})$ added to a given volume of solution, ignoring any subsequent chemical change. Figure 3 shows spectra obtained at the different concentrations; the vertical axis is the "analytical extinction coefficient" based on the analytical concentration of the dimer. The isosbestic points indicate that only two absorbing species are present in solution, lending support to the assumption that radicals and dimers thereof are involved in the equilibrium. However, Figure 3 shows that no wavelength can be chosen whose absorption can be exclusively ascribed to either $C_6S_8^{-\bullet}$ or $C_{12}S_{16}^{2-}$. Therefore, a graphical deconvolution scheme was used, as described in Supporting Information. The calculated equilibrium constant from the deconvolution is

$$K_{eq}\,(\text{THF soln}) = [C_6S_8^{-\bullet}]^2/[C_{12}S_{16}^{2-}] = 1.2 \times 10^{-4}\ \text{M} \quad (4)$$

EPR and Magnetic Susceptibility Measurements on $C_6S_8^{-\bullet}$. Evidence for a dimer−monomer equilibrium in $[C_6S_8]^{n-}{}_n$ also comes from EPR measurements. One would expect the $C_6S_8^{-\bullet}$ monomer to be EPR-active and the $C_{12}S_{16}^{2-}$ dimer to be EPR-silent; therefore, the spin concentration would be less than double the analytical concentration of $(Ph_4P)_2(C_{12}S_{16})$. The concentration of $C_6S_8^{-\bullet}$ was determined by double integration of the experimental spectra, an example of which is shown in Figure 4. The stable radical diphenylpicrylhydrazide (DPPH) was used as an external standard. In THF solutions whose analytical concentration of $(PPh_4)_2(C_{12}S_{16})$ was 1.54×10^{-3} M, the spin concentration, $[C_6S_8^{-\bullet}]$, is 6.01×10^{-4} M. This leads to a K_{eq} of 2.9×10^{-4} M in THF at 17 °C. Some experimental parameters in EPR spectroscopy that are critical to the determination of spin concentration are difficult to control, leading to errors in spin concentration. For this reason, we think that the lower K_{eq} value based on optical spectroscopy is more reliable.

Efforts were made to record the EPR spectrum of a frozen solution containing $(PPh_4)_2(C_{12}S_{16})$; however, at −178 °C, the EPR signal essentially disappears. We attribute this behavior to a monomer−dimer equilibrium that favors the EPR-silent dimer at low temperature. The intensity of the EPR signal was studied as a function of temperature for a solution of a known concentration, and the K_{eq} for the dimer−monomer equilibrium was calculated for the different temperatures. A linear relationship was found between $\ln(K_{eq})$ and T^{-1} (Figure 5), allowing ΔH and ΔS to be determined ($+51.5 \pm 0.5$ kJ mol^{-1} and $+110 \pm 3$ J mol^{-1} K^{-1}, respectively). The intensity of the EPR signal for solutions of $(PPh_4)_2(C_{12}S_{16})$ was also highly solvent-dependent. At concentrations in THF solution where the radical comprises 66% of the solution species, the corresponding DMSO solutions have only 2% of the free radical.

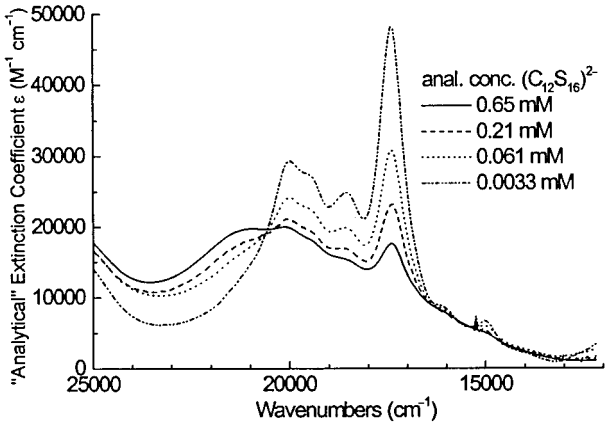

Figure 3. Optical spectra of $(PPh_4)C_6S_8$ in THF solution at concentrations of 0.65, 0.21, 0.061, and 0.0033 mM. The signal at 17 400 cm^{-1} is assigned to $C_6S_8^{-}$.

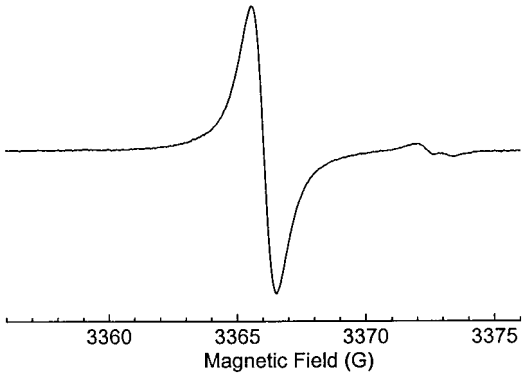

Figure 4. X-band EPR spectra of a 1.54×10^{-3} M THF solution of $(PPh_4)_2C_{12}S_{16}$ at 17 °C ($g_{solution} = 2.0213(7)$).

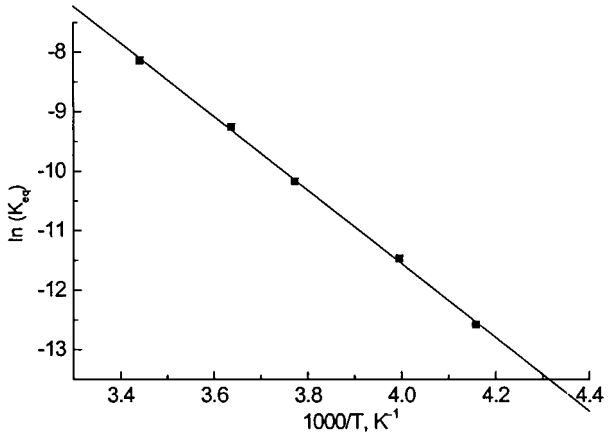

Figure 5. Plot of $\ln(K_{eq})$ vs inverse temperature, where K_{eq} is the equilibrium constant of the splitting of the dimer, $(Ph_4P)_2(C_{12}S_{16})$, into radicals in THF solution. The analytical concentration of the dimer was 1.54×10^{-3} M. The line indicates the linear fit.

Microcrystalline samples of $(PPh_4)_2(C_{12}S_{16})$ show a rhombic signal in the X-band EPR spectrum. Simulation of this spectrum gave $g_x = 2.0413$, $g_y = 2.0103$, and $g_z = 2.0022$ (Figure 6). No hyperfine interactions were observed. Although the EPR measurements established the presence of a paramagnetic species, magnetic susceptibility measurements show that polycrystalline $(PPh_4)_2(C_{12}S_{16})$ is diamagnetic. The positive linear slope of a plot of the magnetic susceptibility vs magnetic field over a range of −7 to +7 T establishes the diamagnetism. We reconcile the observation of an EPR signal for microcrys-

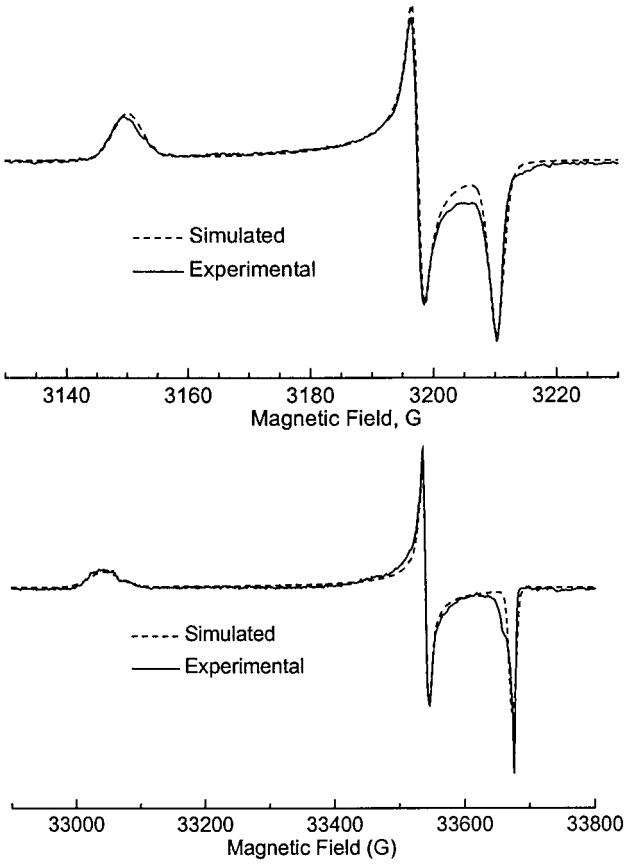

Figure 6. EPR spectra of polycrystalline $(PPh_4)_2(C_{12}S_{16})$ at X-band (top) and W-band (bottom).

talline $(PPh_4)_2(C_{12}S_{16})$ with its bulk diamagnetism by proposing that small amounts of $(PPh_4)(C_6S_8)$ crystallize with $(PPh_4)_2$-$(C_{12}S_{16})$.

Preparation and Structure of $C_6S_{10}^{2-}$. The observation of intemediate oxidation states for the $C_6S_8^{2-/0}$ system encouraged a corresponding investigation of the intermediate redox states of $C_3S_5^{2-/0}$. We obtained red-orange crystals of the one-electron-oxidized product, $(Me_4N)_2(C_6S_{10})$, by the treatment of $(C_3S_5)_n$ with 1 equiv of $(Me_4N)_2(C_3S_5)$ followed by crystallization with ether:

$$^1/_n(C_3S_5)_n + (Me_4N)_2(C_3S_5) \rightarrow (Me_4N)_2(C_3S_5)_2 \qquad (5)$$

The dianion $C_6S_{10}^{2-}$ features C_3S_5 units linked by an S−S bond (Figure 7). The C_3S_5 subunits are unremarkable; that is, the bond distances and angles are quite comparable to those of $(Me_4N)_2$-(C_3S_5) (see below for a discussion of the structure of $C_3S_5^{2-}$ itself). The carbon−carbon bond in $(C_6S_{10})^{2-}$ is 0.02 Å shorter than in $C_3S_5^{2-}$ (vide infra), but other than that, there are no significant differences between the two C_3S_5 units. However, as with $C_{12}S_{16}^{2-}$ (vide supra), the S−S bond length of 2.136 Å is rather long. Furthermore, the torsion angle is unusually acute (51.9°). Selected angles and distances for $(Me_4N)_2(C_6S_{10})$ are shown in Table 2.

Additional insights into the redox properties of $(Me_4N)_2$-(C_6S_{10}) and $(Me_4N)_2(C_3S_5)$ were sought using cyclic voltammetry. The cyclic voltammogram of $C_6S_{10}^{2-}$ shows a rest potential of −0.6 V (vs Fc^+/Fc) and a broad, cathodic quasi-reversible peak (Figure 8) whose potential is significantly dependent (−1.52 V for Au, −1.66 V for Pt, and −1.59 V for C) on the electrode material. These waves are assigned according

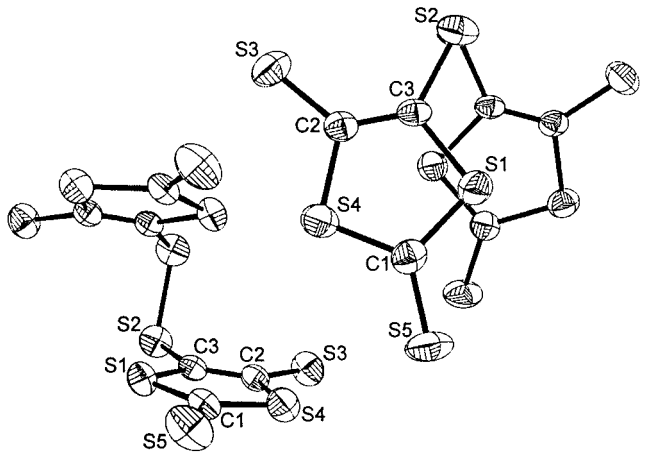

Figure 7. Molecular structure of the anion, $C_6S_{10}^{2-}$, crystallized as its NMe_4^+ salt, shown in two orientations with thermal ellipsoids drawn at the 50% probability level.

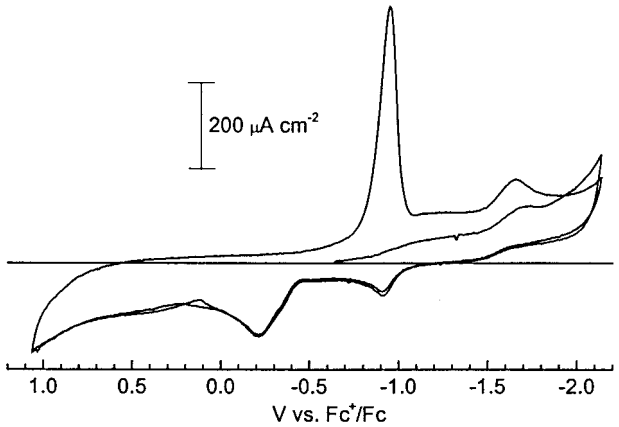

Figure 8. Cyclic voltammogram of $(Me_4N)_2(C_6S_{10})$, 1×10^{-3} M in acetonitrile: electrolyte, 0.1 M Bu_4NPF_6; working electrode, Pt; scan rate, 0.1 V/s. Potentials are referenced to Fc^+/Fc.

Table 2. Selected Angles (deg) and Distances (Å) for the Anion in $(Me_4N)_2(C_6S_{10})$

S(1)−C(1)	1.719(6)	S(4)−C(2)	1.768(6)
S(1)−C(3)	1.764(6)	S(5)−C(1)	1.651(6)
S(2)−C(3)	1.733(6)	C(2)−C(3)	1.350(7)
S(2)−S(2a)	2.135(4)	C(3)−S(2)-S(2a)	102.4(2)
S(3)−C(2)	1.687(6)	C(2)−C(3)−S(2)	127.3(5)
S(4)−C(1)	1.730(6)	C(3)−S(2)−S(2a)−C(3a)	52.1

to the following equation (potentials given for the Pt electrode):

$$C_3S_5^{2-} \underset{E_c = -1.66\ V}{\overset{E_a = -0.90\ V}{\rightleftharpoons}} (C_3S_5)_2^{2-} \underset{E_c = -0.95\ V}{\overset{E_a = -0.21\ V}{\rightleftharpoons}} (C_3S_5)_n^{2-} \qquad (n > 2) \quad (6)$$

The sluggishness of this process is fairly typical of the redox properties of organic disulfides, which often exhibit slow electrode kinetics.[17] This reduction is coupled to an anodic peak at −0.90 V vs Fc^+/Fc; the potential for the anodic peak was not found to vary with the electrode material. In the cyclic voltammogram of $C_3S_5^{2-}$, the rest potential is −1.1 V, with an anodic peak at −0.90 V, which is coupled to a very broad, cathodic peak starting at about −1.0 V. From the similarity of the oxidative behavior of $C_3S_5^{2-}$ and the reoxidation of the reduction product of $C_6S_{10}^{2-}$, we conclude that the reduction product of $C_6S_{10}^{2-}$ is $C_3S_5^{2-}$. Furthermore, $C_3S_5^{2-}$ appears to

(17) Persson, B. *J. Electroanal. Chem.* **1978**, *86*, 313.

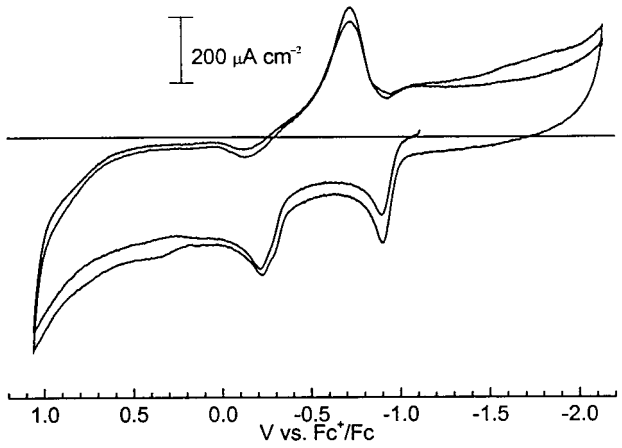

Figure 9. Cyclic voltammogram of $(NMe_4)_2C_3S_5$, 1×10^{-3} M in acetonitrile: electrolyte, 0.1 M Bu_4NPF_6; working electrode, glassy carbon; scan rate, 0.1 V/s. Potentials are referenced to Fc^+/Fc.

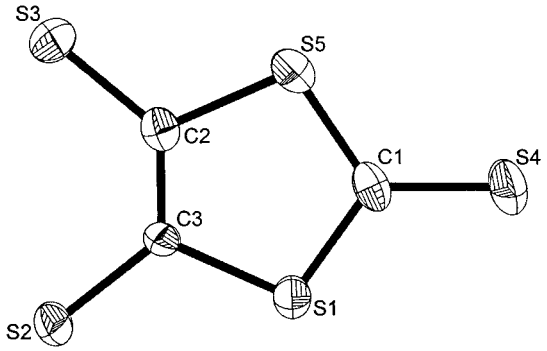

Figure 10. Molecular structure of the anion in $(NMe_4)_2(C_3S_5)$ with thermal ellipsoids drawn at the 50% probability level.

be electrochemically oxidized much more quickly than it is rereduced (Figure 9). An anodic peak appears at −0.2 V corresponding to the oxidation of $C_6S_{10}^{2-}$. This anodic process is coupled to a stripping peak whose potential is dependent on the electrode material; the rereduction is easier on a gold electrode (−0.90 V) than on platinum (−0.95 V) or glassy carbon (−0.98 V). It is likely that this stripping peak corresponds to the rereduction of $(C_3S_5)_n^{2-}$ oligomers.

Structure of $C_3S_5^{2-}$. Although a great number of organic derivatives and metal (especially nickel) complexes of $C_3S_5^{2-}$ have been crystallographically characterized,[18] the structure of an uncomplexed, underivatized $C_3S_5^{2-}$ salt has not been reported. $(Me_4N)_2(C_3S_5)$ is sparingly soluble in acetonitrile, and blue crystals of the acetonitrile solvate were grown both by evaporation or by layering with ether. The structure is shown in Figure 10, and the bond lengths are shown in Table 3. No evidence of hydrogen bonding is observed.

Discussion

Figure 11 shows a scatter plot of S−S bond lengths vs CS−SC torsion angles, as gathered from the Cambridge Structural Database (version 5.18, 1999).[19] The plot excludes all structures whose S−S unit is part of a ring. The largest density of data

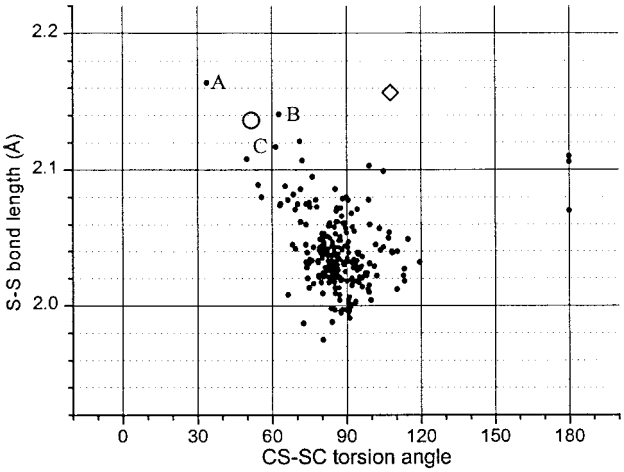

Figure 11. S−S bond lengths vs CS−SC dihedral angles for crystallographically characterized organic disulfides whose disulfide unit is not part of a ring.

Table 3. Selected Angles (deg) and Distances (Å) for the Anion in $(Me_4N)_2(C_3S_5)$

S(1)−C(1)	1.689(6)	C(2)−C(3)−S(2)	127.8(5)
S(1)−C(3)	1.759(6)	C(2)−C(3)−S(1)	114.8(4)
S(2)−C(3)	1.727(6)	S(2)−C(3)−S(1)	117.4(3)
S(3)−C(2)	1.721(6)	S(4)−C(1)−S(1)	125.0(4)
S(4)−C(1)	1.675(6)	S(4)−C(1)−S(5)	124.1(4)
S(5)−C(1)	1.733(7)	S(1)−C(1)−S(5)	110.9(3)
S(5)−C(2)	1.775(6)	C(1)−S(1)−C(3)	100.9(3)
C(2)−C(3)	1.371(8)	C(1)−S(5)−C(2)	99.8(3)
C(3)−C(2)−S(5)	113.5(5)	C(3)−C(2)−S(3)	129.7(5)
S(3)−C(2)−S(5)	116.7(4)		

points is concentrated in the bond length region between 2.00 and 2.06 Å, with the torsion angles between 75° and 90°. MO calculations suggest that CS−SC dihedral angles near 90° are stabilized by a weak bonding interaction between the C−S σ^* orbital located on one sulfur atom and the $3p_z$ lone pair on the other sulfur atom.[20]

Figure 11 shows three structures whose C−S−S−C dihedral angles are 180°. This angle may be attributed to the sterically demanding substituents. An example of a compound with such substituents is tris(trimethylsilyl)methyl disulfide.[21] No acyclic structures have dihedral angles of zero (although many cyclic ones do). A number of disulfides have rather acute dihedral angles; however, none have dihedral angles between 120° and 180°. As can be seen on the plot, longer S−S bond lengths correlate with more acute dihedral angles. Although the general trend is informative, it is also useful to consider a few of the points representing structures possessing long S−S bonds and acute torsion angles. Three such structures are shown in Chart 1, and in the scatter plot, as compounds **A**,[22] **B**,[23] and **C**.[24] These

(18) (a) Takamatsu, N.; Akutagawa, T.; Hasegawa, T.; Nakamura, T.; Inabe, T.; Fujita, W.; Awaga, K. *Inorg. Chem.* **2000**, *39*, 870. (b) Akutagawa, T.; Nakamura, T.; Inabe, T.; Underhill, A. E. *J. Mater. Chem.* **1997**, *7*, 183. (c) Nakamura, T.; Akutagawa, T.; Honda, K.; Underhill, A. E.; Coomber, A. T.; Friend, R. H. *Nature* **1998**, *394*, 159. (d) Malfant, I.; Andreu, R.; Lacroix, P. G.; Faulmann, C.; Cassoux, P. *Inorg. Chem.* **1998**, *37*, 3361.

(19) The database is the Cambridge Structural Data Centre, http://www.ccdc.cam.ac.uk/. In the search, all structures containing the C−S−S−C unit were included except those where the S−S bond is part of a ring.

(20) (a) Steudel, R.; Drozdova, Y.; Miaskiewicz, K.; Hertwig, R. H.; Koch, W. *J. Am. Chem. Soc.* **1997**, *119*, 1990. (b) Alleres, D. R.; Cooper, D. L.; Cunningham, T. P.; Gerratt, J.; Karadakov, P. B.; Raimondi, M. *J. Chem. Soc., Faraday Trans.* **1995**, *91*, 3357. (c) Aida, M.; Nagata, C. *Theor. Chim. Acta* **1986**, *70*, 73.

(21) Ostrowski, M.; Jeske, J.; Jones, P. G.; duMont, W.-W. *Chem. Ber.* **1993**, *126*, 1355.

(22) Alajarin, M.; Molina, P.; Perez, M. J.; Concepción, M.; Hernández, F.; Claramunt, R. M.; Elguero, J. *Chem. Scr.* **1985**, *25*, 230.

(23) Yufit, D. S.; Struchkov, Y. T. *Izv. Akad. Nauk SSSR, Ser. Khim.* **1985**, 2724.

(24) Jagodziński, T. S.; Sośnicki, J.; Jagodzińska, E.; Królikowska, M. *J. Prakt. Chem.* **1996**, *338*, 578.

Chart 1

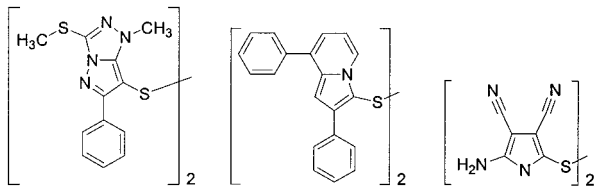

A B C

disulfides have torsion angles of 33.9°, 62.8°, and 61.6° and S−S bonds of 2.164, 2.141, and 2.117 Å, respectively.

The R subunits for all three of these RS−SR compounds display a significant degree of aromaticity. In the crystal, the S−S bonds for these molecules are twisted such that the aromatic units lie on top of each other for favorable $\pi-\pi$ interactions. But these aromatic interactions come at an energetic price when the S−S bond is considered. As described above, the ideal torsion angle of the S−S bond is about 90° due to favorable overlap between the C−S σ^* and the lone pair on sulfur.[20] When this overlap is no longer geometrically possible, the bond weakens, resulting in a longer S−S distance. Note that **A** in Chart 1 represents the longest crystallographically characterized bond between divalent sulfur in an acyclic system.

Van Wart et al. carried out a study in 1973, based on the limited number of crystallographically characterized species found at the time, of the relationship between CS−SC dihedral angles and both the Raman S−S stretching frequency and the UV cutoff.[25] Their results may be regarded as a confirmation of the trend in Figure 11: An acute dihedral angle is associated with a lower ν_{S-S} and a lower-energy UV cutoff.[26] Both of these trends point to a weaker (longer) S−S bond that is based on ν_{S-S} correlating with the expected relationship between bond strength and stretching frequency and that with the UV cutoff correlating with the assumption that this absorption is due to the S−S $\sigma \rightarrow \sigma^*$ transition.

The long S−S bond in $C_{12}S_{16}^{2-}$ is, however, not explained by the correlation shown by van Wart and Figure 11. The data for $C_{12}S_{16}^{2-}$ are shown by the diamond in Figure 11. Although the S−S bond is longer than that of any other disulfide in Figure 11, with the exception of compound **A**, the associated dihedral angle is not acute as expected on the basis of the trend. Additionally, as can be seen in Figure 2, the two $C_6S_8^-$ subunits are not stacked on top of each other. Therefore, the explanation for the unusually long S−S bond in $C_{12}S_{16}^{2-}$ is the result of a previously unrecognized effect. The possibility of lowered bond orders due to hypervalent sulfur atoms may be discounted; contacts between the (formal) thiolate sulfur on one $C_{12}S_{16}^{2-}$ anion and the disulfide sulfur on the other are 3.433 Å long, which is slightly shorter than twice the covalent radius of the sulfur atom.[27] However, this contact is still quite long and is likely unimportant; the sulfur atoms in the S−S bond are not hypervalent.

Therefore, π-delocalization (aromaticity) appears to be a useful explanation for the long S−S bond in $C_{12}S_{16}^{2-}$. It was noted above that C_6S_8 undergoes two one-electron reductions at potentials that are quite close to each other, despite the charge loading on the reduced species.[28] This means that the C_6S_8 unit acts as a molecular capacitor: the charge on the $C_6S_8^-$ subunit is not localized on the thiyl sulfur atom but is delocalized as found for other stable free radicals. The long S−S bond also correlates with the tendency of $C_{12}S_{16}^{2-}$ to homolytically dissociate.

Considering once again the scatter plot between CS−SC torsion angle and S−S bond length, one can place the corresponding data for $(C_6S_{10})^{2-}$ on this plot, as represented by the circle in Figure 11. It can be seen that even though the S−S bond is rather long, it is of an expected length considering the CS−SC torsion angle. Unlike in the case of $C_{12}S_{16}^{2-}$, $C_6S_{10}^{2-}$ does appear to be in line with the trend with increasing S−S bond length with more acute torsion angle. Additionally, just as $C_6S_{10}^{2-}$ falls within the trend made by other disulfides, both geometric parameters can be explained with the same phenomenon exhibited by other disulfides with acute torsion angles: π-stacking. This intramolecular interaction, as explained above, twists the CS−SC subunit from the geometry required for ideal orbital overlap, lengthening the S−S bond.

The structure of $(Me_4N)_2(C_3S_5)$ bears mentioning because it is the first time this versatile ligand has been crystallographically characterized when not coordinated or derivatized. The most basic atoms on the anion are expected to be the thiolate sulfur atoms, yet the nearest S···H contact is 2.76 Å, and that is to a Me_4N^+ hydrogen; therefore, the $C_3S_5^{2-}$ anion may be regarded as well isolated from any Lewis acids. Our success in isolating the free anion as a quaternary ammonium salt may be explained by the finding that $C_3S_5^{2-}$ is an exceptionally weak Bronsted base when compared with other dithiolenes: the pK_a of $HC_3S_5^-$ in water is 5.31.[29] As in some comparisons, the ethene-1,2-dithiolate ion (monoprotonated) has a pK_a of 12.13, and even monoprotonated 1,2-dicyanoethene-1,2-dithiolate, with the electron-withdrawing substituents lowering the basicity, has a pK_a value of 7.55.[30] Because the anion in $(Me_4N)_2C_3S_5$ is well isolated, it is useful to compare the structure of this $C_3S_5^{2-}$ anion with its derivatives. For example, a Cambridge Structural Database search of structures containing the NiC_3S_5 fragment turned up 201 fragments in 66 structures, which were predominantly $[Ni(C_3S_5)_2]^{n-}$ salts. The lengths of the formal carbon−carbon double bond ranged between 1.31 and 1.42 Å. Within this wide range though, the greatest number of fragments (36) were found in the range between 1.370 and 1.378 Å, which matches the carbon−carbon distance in $(Me_4N)_2C_3S_5$ itself (1.371 Å).

The structure of $C_{12}S_{16}^{2-}$ has been shown in this paper. Previously,[12] we have described the structure of $C_6S_8^{2-}$ and inferred the structure of C_6S_8 (eq 1) from that of its derivative, $C_6S_6O_2$. The structure of $C_6S_8^{-\bullet}$ has not been determined because of its tendency to dimerize in the solid phase. However, the known chemistry of organic sulfur-centered radicals can be used to postulate a structure for $C_6S_8^{-\bullet}$. Thiyl radicals, RS$^\bullet$, will react with thiolates to give a disulfide radical anion with a three-electron bond.[31] Additionally, thioethers, when oxidized by a suitable oxidant such as the hydroxyl radical, will form an intermolecular three-electron S−S bond to form a radical cation, $(R_2S)_2^{+\bullet}$.[32] One can therefore envision the oxidation of $C_6S_8^{2-}$

(25) Van Wart, H. E.; Lewis, A.; Scheraga, H. A.; Saeva, F. D. *Proc. Natl. Acad. Sci.* **1973**, *10*, 2619.
(26) It should be noted that Van Wart et al. included in their work disulfides that are part of a ring. Some, as one would expect, possessed CS−SC dihedral angles that are much more acute than those found in Figure 11. Nevertheless, even the disulfides that were part of a ring followed the trends observed by the authors.
(27) (a) Huheey, J. E.; Keiter, E. A.; Keiter, R. L. *Inorganic Chemistry*; Harper Collins: New York, 1993. (b) *CRC Handbook of Chemistry and Physics*; CRC Press: Boca Raton, FL, 1987.
(28) Persson, B. *J. Electroanal. Chem.* **1978**, *86*, 313.
(29) Breitzer, J. G. Ph.D. Thesis, University of Illinois at Urbana−Champaign, Urbana, IL, 2000.
(30) Schmidt, S.; Dietze, F.; Jokuszies, A.; Zeltner, S.; Olk, R.-M.; Reinhold: J.; Hoyer, E. *Sulfur Lett.* **1995**, *19*, 119.
(31) Mezyk, S. P. *J. Phys. Chem.* **1996**, *100*, 8861−8866.
(32) Asmus, K.-D. *Acc. Chem. Res.* **1979**, *12*, 6.

to give a species where one sulfur is a thiolate and the other a thiyl radical. These will then react intramolecularly in the same manner in which organic thiyl radicals and thiolates react intermolecularly:

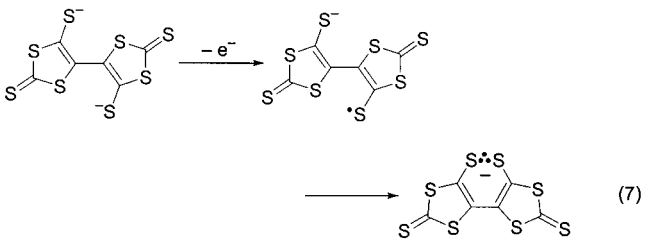

(7)

As reviewed by Asmus, the strength of the S−S bond in reduced disulfides increases with the electronegativity of the substituents. The electron-withdrawing character of the carbon sulfide framework is indicated by the positive reduction potentials for C_6S_8 of 0.331 and 0.181 V (vs NHE).

Summary

Optical, magnetic, and EPR measurements show that paramagnetic $C_6S_8^-$ and diamagnetic $C_{12}S_{16}^{2-}$ exist in equilibrium (eq 7). For the radical, $C_6S_8^-$, we propose a tricyclic structure with the unpaired electron delocalized throughout the π-system, as suggested by the nonobservation of hyperfine coupling to ^{33}S.[33] Equilibrium measurements evaluated by EPR spectroscopy indicate that this odd-electron species, while abundant in dilute solution, is less stable than the S−S coupled dimer, $C_{12}S_{16}^{2-}$, at the higher concentrations used in the synthesis. The enthalpy of dimerization is -51.5 kJ mol^{-1}.

The redox properties of $C_3S_5^{2-}$ proved to be particularly insightful. The reaction of $C_3S_5^{2-}$ with C_3S_5 to give $C_6S_{10}^{2-}$ is analogous to the reaction of the sulfide ion with sulfur to give the persulfide ion. To extend this analogy, one can conceive of higher oligomers of $(C_3S_5)_n^{2-}$ ($n > 2$), which would be analogous to polysulfide ions. These would consist of C_3S_5 units linked through S−S bonds, and these structures would be consistent with our previous suggestion[1] of a polymeric structure for $(C_3S_5)_n$.

Experimental Section

Materials and Methods. All reagents and inorganic salts were used as received while solvents were dried and deoxygenated by standard methods. The following species have been previously reported: $C_3S_5(C(O)Ph)_2$,[34] C_6S_8,[35] $Cs_2C_3S_5$,[36] and $(C_3S_5)_n$.[35] ^{13}C NMR measurements were recorded on a Varian-Oxford 500 MHz NMR spectrometer. ^{13}C NMR resonances for the PPh_4^+ cation were observed at δ 117.6 (d), 130.5 (d), 134.5 (d), and 135.4 (d). IR spectra were recorded on KBr disks and are reported in cm^{-1}. IR absorptions for the PPh_4^+ cation are seen in all samples at 527, 688, 722, 750, 942, 1107, and 1439 cm^{-1}. Electrochemical measurements were conducted using a glassy carbon working electrode, a Pt counter electrode, and a saturated silver chloride electrode (SSCE) in 0.1 M Bu_4NPF_6 in DMF. Cyclic voltammetry measurements were measured at a scan rate of 100 mV/s.

UV−vis spectra of various concentrations of the radical/dimer equilibrium mixture, $C_6S_8^-/C_{12}S_{16}^{2-}$, were collected in THF. To allow measurable absorptions, cuvettes of path lengths of 0.1, 0.3, 1.0, and 10 cm were used, the shortest path length being used for the most concentrated solution.

Electron Paramagnetic Resonance Spectroscopy. EPR spectra at X-band (9.0 GHz) were recorded with a Varian (Palo Alto, CA) Century series E-112 spectrometer equipped with a Varian TE102 cavity. Microwave power and 100 kHz modulation amplitude were chosen in such a way as to avoid line shape distortion. The magnetic field was calibrated by a tracking NMR gauss meter (Varian, model 92980102P). Microwave frequency was measured by an on-line frequency counter (Systron Donner, model 6016, Concord, CA). Data acquisition was carried out by means of an IBM personal computer with an IBM analog−digital card, running a commercial software package (Scientific Software Services, Bloomington, IL). DMF and THF solutions were drawn into sufficiently narrow (1 mm i.d.) quartz capillaries (VitroCom, Inc., Mountain Lakes, NJ) to minimize absorptions from the solvent. The W-band (94 GHz) spectrometer at the University of Illinois EPR Research Center is described elsewhere.[37]

The concentration of paramagnetic species in THF solvent was determined by comparing the double integrals of their EPR spectra with those of a reference sample with a known spin concentration. This reference sample was prepared by dissolving a weighed amount of 2,2-di(4-tert-octylphenyl)-1-picrylhydrazyl (DPPH, 98%, Aldrich) in the appropriate solvent, in the same capillary size as the experimental samples. Line shape analysis of solution EPR spectra was carried out by a computer program based on a fast convolution algorithm with a Levenberg−Marquardt optimization method.[38]

There are some sources of systematic error in concentrations as measured by EPR spectroscopy. One of these is nonresonant absorption of the microwave radiation by the solvent. This absorption increases with dielectric constant and also depends on the sample geometry. This error due to solvent dielectric losses was minimized by dissolving the DPPH in the same solvent as that used for the sample (THF) and by attemping to match the geometries (sample tube sizes, placement in the cavity) between the standard and the sample.

The variable temperature EPR measurements from −33 to 17 °C were carried out using a standard Varian variable temperature accessory. However, the temperature dependence of the dielectric constant of the solvent (THF) could potentially affect the signal intensity. The absence of this effect was confirmed by measuring the double integral of the DPPH standard at 20 and at −40 °C; the signal intensities were within 2% of each other after allowing for the Curie law.

Synthesis of $(PPh_4)_2(C_6S_8)$. A dark-purple suspension of 0.328 g (1 mmol) of C_6S_8 in 30 mL of THF was cooled with an acetone−dry ice bath and treated dropwise with 2.2 mL of a 1 M THF solution of $LiBHEt_3$. A homogeneous violet-red solution resulted almost immediately. The THF was removed under vacuum, and 50 mL of O_2-free H_2O was added to redissolve the dark-brown residue. A solution of 0.75 g (2 mmol) of PPh_4Cl in 30 mL of O_2-free H_2O was added to the dark-brown solution to give violet microcrystals. The crude solid was washed with water and dried under vacuum. Yield: 0.985 g (98%). Alternatively, the reduction of the C_6S_8 can be achieved by using Na metal in liquid NH_3. IR (KBr): 1365 and 1024 ($\nu_{C=S}$) cm^{-1}. ^{13}C NMR (DMF): δ 207.3 (s), 159.2 (s), and 123.7 (s). Anal. Calcd for $C_{54}H_{40}P_2S_8$: C, 64.41; H, 3.97; S, 25.47. Found: C, 64.70; H, 3.99; S, 25.11.

Synthesis of $(PPh_4)(C_6S_8)$. An amalgam was prepared by adding 0.047 g (2.04 mmol) of Na to 30 g of Hg. After being washed with two 10 mL portions of THF, the amalgam was treated with 10 mL of THF and 0.101 g (0.307 mmol) of C_6S_8. The mixture was stirred at ambient temperature for 30 min, during which time the brown suspension became red. This mixture was decanted from the amalgam and filtered through Celite. The red filtrate was then treated with an additional 0.102 g (0.309 mmol) of C_6S_8 and 0.239 g (0.638 mmol) of

(33) Sullivan, P. D. *J. Am. Chem. Soc.* **1968**, *90*, 3618.
(34) Steimecke, G.; Sieler, H.-J.; Kirmse, R.; Hoyer, E. *Phosphorus Sulfur Relat. Elem.* **1979**, *7*, 49.
(35) Galloway, C. P.; Doxsee, D. D.; Fenske, D.; Rauchfuss, T. B.; Wilson, S. R.; Yang, X. *Inorg. Chem.* **1994**, *33*, 4537.
(36) Gasiorowski, R.; Jorgensen, T.; Moller, J.; Hansen, T. K.; Pietraszkiewicz, M.; Becher, J. *Adv. Mater.* **1992**, *4*, 568.
(37) Wang, W.; Belford, R. L.; Clarkson, R. B.; Davis, R. B.; Forrer, R. B.; Nilges, M. J.; Timken, M. D.; Watczak, T.; Thurnauer, M. C.; Norris, J. R.; Morris, A. L.; Zwang, Y. *Appl. Magn. Res.* **1994**, *6*, 195.
(38) (a) Smirnov, A. I.; Belford, R. L. *J. Magn. Reson. A* **1995**, *98*, 65. (b) Smirnov, A. I.; Clarkson, R. B.; Belford, R. L. *J. Magn. Reson. B* **1996**, *111*, 149.

Table 4. Crystallographic Data for $(Me_4N)_2(C_3S_5)\cdot CH_3CN$, $(Me_4N)_2(C_6S_{10})$, and $(Ph_4P)_2(C_{12}S_{16})$

	$(Me_4N)_2(C_3S_5)\cdot CH_3CN$	$(Me_4N)_2(C_6S_{10})$	$(Ph_4P)_2(C_{12}S_{16})$
empirical formula	$C_{13}H_{27}N_3S_5$	$C_7H_{12}NS_5$	$C_{60}H_{40}P_2S_{16}$
fw	385.68	270.48	1335.82
cryst syst	orthorhombic	monoclinic	triclinic
space group	$P2_12_12_1$ (No. 19)	$C2/c$ (No. 15)	$P\bar{1}$ (No. 2)
temp (K)	193(2)	193(2)	198(2)
θ range for data collection (deg)	1.83−28.28	2.11−23.24	1.19−16.50
data/restraints/parameters	4978/0/190	1819/0/122	3145/0/299
cryst size (mm)	0.08 × 0.08 × 0.42	0.03 × 0.06 × 0.10	0.03 × 0.03 × 0.54
λ (Å)	0.710 73	0.710 73	0.710 73
a (Å)	7.8369(7)	17.345(3)	12.752(2)
b (Å)	11.9139(11)	11.6871(18)	14.787(2)
c (Å)	22.278(2)	12.727(2)	18.433(3)
α (deg)	90	90	68.711(2)
β (deg)	90	100.329(4)	80.516(3)
γ (deg)	90	90	68.458(2)
V (Å^3)	2080.1(3)	2538.1(7)	3010.5(7)
Z	4	8	2
ρ_{calcd} (g/cm^3)	1.232	1.416	1.474
μ (cm^{-1})	5.55	8.72	6.67
R^a [$I > 2\sigma(I)$]	0.0747	0.0523	0.1472
R (all data)	0.1377	0.1823	0.3275
GOF	0.974	0.804	1.016

[a] $R = \sum||F_o| - |F_c||/\sum|F_o|$.

Ph_4PCl. Within ∼1 min, the red color of the mixture changed to deep brown. The mixture was stirred at room temperature for 3.5 h to allow ion exchange to occur. The brown mixture was then filtered through Celite directly into 100 mL of Et_2O, which resulted in a brown powder. Yield: 0.195 g (48%). Anal. Calcd for $C_{60}H_{40}P_2S_{16}$: C, 53.95; H, 3.02. Found: C, 54.12; H, 3.38. IR (KBr): 3050, 1482, 1436, 1186, 1106, 1050, 894, 722, 686, 526, 454 cm^{-1}. UV−vis (THF): λ_{max}/nm (ϵ/M^{-1} cm^{-1}) 500 (24 000), 540 (19 600), 576 (30 500) at 6.1 × 10^{-5} M, 1 cm path length. Concentration is specified because of the deviation from Beer's law.

Synthesis of $(Me_4N)_2(C_3S_5)$. A solution of NaOMe prepared from 0.20 g (8.7 mmol) of Na and 16 mL of MeOH was treated with 0.3262 g (0.8023 mmol) of $C_3S_5[C(O)Ph]_2$. Solvent was removed from the resulting red $Na_2C_3S_5$ solution, and the methyl benzoate byproduct was removed by washing the pink solid with three 10 mL portions of CH_2Cl_2. The solid was extracted with 16 mL of MeCN, resulting in a purple solution and undissolved NaOMe. This slurry was treated with 0.1765 g (1.61 mmol) of Me_4NCl, causing the solution color to become blue. The NaOMe and NaCl were removed by filtration, and 30 mL of Et_2O was added to precipitate blue crystals of $(Me_4N)_2C_3S_5\cdot$MeCN. Crystals suitable for X-ray diffraction were grown by layering a MeCN solution of $(Me_4N)_2C_3S_5$ with Et_2O. IR (KBr): 3000, 1482, 1372, 1022, 948, 458 cm^{-1}. UV−vis (MeCN): λ_{max}/nm (ϵ/M^{-1} cm^{-1}) 582 (3000).

Synthesis of $(Me_4N)_2(C_6S_{10})$. A solution of 0.0437 g (0.113 mmol) of $(Me_4N)_2(C_3S_5)\cdot$MeCN in 2.5 mL of MeCN was treated with 0.0221 g (0.113 mmol) of C_3S_5. The blue solution assumed an orange-red color within 10 min. The solution was added to ∼20 mL of Et_2O, resulting in a powder, and ∼3 mL MeCN was added until the powder became more crystalline. Yield: 0.024 g (39%). Anal. Calcd for $C_{14}H_{24}N_2S_{10}$: C, 31.08; H, 4.47; N, 5.18. Found: C, 30.83; H, 4.62; N, 4.87. IR (KBr): 3010, 1480, 1366, 1034, 946, 864, 464 cm^{-1}. λ_{max}/nm (ϵ/M^{-1} cm^{-1}) 478 (8000).

Crystallographic Analysis of $(Ph_4P)_2(C_{12}S_{16})$. X-ray quality crystals of $(PPh_4)_2(C_{12}S_{16})$ were obtained from THF/hexanes solutions at 25 °C. A black, columnar crystal for analysis was attached to a thin glass fiber with Paratone-N oil (Exxon). The data crystal was bound by the (1 1 1), (−1 −1 −1), (−1 0 1), (1 0 −1), (0 −1 0), and (0 1 0) faces. Distances from the crystal center to these facial boundaries were 0.270, 0.270, 0.015, 0.015, 0.015, and 0.015 mm, respectively. Data were collected at 198 K on a Siemens CCD diffractometer. Crystal and refinement details are given in Table 4. Systematic conditions suggested the unambiguous space group $P\bar{1}$. The structure was solved by direct methods using SHELXTL and refined by full-matrix least-squares refinement on F^2. H atom U's were assigned at 1.2 times the U_{eq}'s of adjacent C atoms. Because of the weak reflections, 2θ was limited to 40°, anisotropic thermal parameters were used for S and P, and isotropic parameters were used for all other atoms. Successful convergence of the least-squares refinements was indicated by the maximum shift per error for the last cycle.

Crystallographic Analysis of $(Me_4N)_2(C_3S_5)$. X-ray quality crystals of $(Me_4N)_2(C_3S_5)$ were obtained from MeCN/Et_2O solutions at 25 °C. A black, columnar crystal for analysis was attached to a thin glass fiber with Paratone-N oil (Exxon). The data crystal was bound by the (0 1 1), (0 −1 −1), (0 1 −1), (0 −1 1), (1 0 1), and (−1 0 −1) faces. Distances from the crystal center to these facial boundaries were 0.040, 0.040, 0.040, 0.040, 0.210, and 0.210 mm, respectively. Data were collected at 193 K on a Siemens CCD diffractometer. Crystal and refinement details are given in Table 4. Systematic conditions suggested the orthorhombic space group $P2_12_12_1$. The structure was solved by direct methods using SHELXTL and refined by full-matrix least-squares refinement on F^2. H atom U's were assigned at 1.2 times the U_{eq}'s of adjacent C atoms. Anisotropic thermal parameters were used on all non-hydrogen atoms. Successful convergence of the least-squares refinements were indicated by the maximum shift per error for the last cycle.

Crystallographic Analysis of $(Me_4N)_2(C_6S_{10})$. X-ray quality crystals of $(Me_4N)_2(C_6S_{10})$ were obtained from MeCN/Et_2O solutions at 25 °C. An orange, platelike crystal for analysis was attached to a thin glass fiber with Paratone-N oil (Exxon). The data crystal was bound by the (1 0 1), (−1 0 −1), (−1 0 1), (1 0 −1), (1 1 0), (−1 −1 0), and (1 −2 −2) faces. Distances from the crystal center to these facial boundaries were 0.015, 0.015, 0.030, 0.030, 0.050, 0.050, and 0.050 mm, respectively. Data were collected at 193 K on a Siemens CCD diffractometer. Crystal and refinement details are given in Table 4. Systematic conditions suggested the monoclinic space group $C2/c$. The structure was solved by direct methods using SHELXTL and refined by full-matrix least-squares refinement on F^2. H atom U's were assigned at 1.2 times the U_{eq}'s of adjacent C atoms. Anisotropic thermal parameters were used on all non-hydrogen atoms. Successful convergence of the least-squares refinements were indicated by the maximum shift per error for the last cycle.

Acknowledgment. This research was supported by NSF and the Department of Energy. L.F.S. thanks NSF for a postdoctoral fellowship. EPR measurements were conducted at the Illinois EPR Research Center, which is supported by NIH P41-RR01811.

Appendix

Following is how the optical data for the equilibrium between $C_6S_8^{-\bullet}$ and $C_{12}S_{16}^{2-}$ were deconvoluted to arrive at an equi-

librium constant. Known was the analytical concentration, C_0, of $(Ph_4P)_2C_{12}S_{16}$ and from this the analytical extinction coefficient, ϵ_{analyt}, at 574 nm. This particular wavelength was chosen because it is the λ_{max} of $C_6S_8^{-\bullet}$ ("radical") and so is the point where the extinction coefficient of the radical is much greater than that of the dimer. Not known were the extinction coefficients of the radical or dimer because neither exists in the absence of the other. To find the equilibrium constant, K_{eq}, the following equilibrium was assumed:

$$C_{12}S_{16}^{2-} \rightleftharpoons 2C_6S_8^{-\bullet} \tag{A1}$$

$$K_{eq} = \frac{[C_6S_8^{-\bullet}]^2}{[C_{12}S_{16}^{2-}]} \tag{A2}$$

First, a guess was made for the value of K_{eq}. Next, by use of this guess, the amount of dimer that dissociates into radicals, x, was determined for each concentration by solving the following expression for K_{eq}:

$$K_{eq} = \frac{(2x)^2}{C_0 - x} \tag{A3}$$

By use of x, the fraction of dimer that dissociated into radicals was determined:

$$f_{rad} = \frac{^1/_2 x}{C_0} \tag{A4}$$

ϵ_{analyt} was then determined from both the measured absorbance and C_0 independently of the guess of K_{eq}:

$$\epsilon_{analyt} = \frac{A}{C_0} \tag{A5}$$

ϵ_{analyt} was then plotted against f_{rad}, and the value of K_{eq} was adjusted until this plot was linear (Figure 12). A linear relationship between f_{rad} and ϵ_{analyt} indicated a correct value of K_{eq} because the contributions to the total analytical extinction coefficient from both the radical and the dimer must depend linearly on their concentrations:

$$A = 2\epsilon_r C_0 f_{rad} + \epsilon_d C_0 (1 - f_{rad}) \tag{A6}$$

where ϵ_r is the extinction coefficient of the radical and ϵ_d is the extinction coefficient of the dimer.

If the guess of K_{eq} were incorrect, ϵ_{analyt} (the y axis in Figure 12) would be unaffected, but the values of f_{rad} (x axis) would be in error in such a way as to make the plot nonlinear. A relatively small (factor of 2) deviation from this equilibrium constant will result in an obviously nonlinear plot. This therefore lends some confidence to the value of K_{eq}:

$$K_{eq}\,(\text{THF soln}) = [C_6S_8^{-}]^2/[C_{12}S_{16}^{2-}] = 1.2 \times 10^{-4}\ \text{M} \tag{A7}$$

Additionally, ϵ_r and ϵ_d can also be determined by extrapolating the linear plot to $f_{rad} = 1$ and 0, respectively. This gives $\epsilon_r = 5.2 \times 10^4$ and $\epsilon_d = 9.5 \times 10^3\ M^{-1}\ cm^{-1}$ at the chosen wavelength of 574 nm.

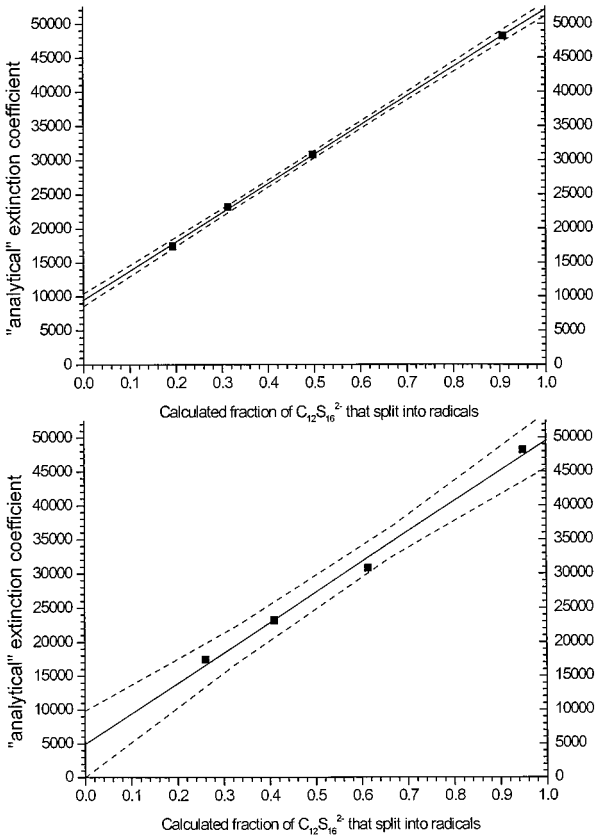

Figure 12. Plot of analytical extinction coefficient (ϵ_{analyt}) versus $[C_6S_8^{-}]$ illustrating the method of deconvoluting optical data for it and its dimer—both absorbing at all wavelengths—to arrive at a dimerization constant. The upper plot shows four data points whose f_{rad} (x-axis) was calculated using $K_{eq} = 1.2 \times 10^{-4}$. The lower plot shows the corresponding data using $K_{eq} = 2.4 \times 10^{-4}$. The solid line is the line of best fit, and the dotted lines are the 90% confidence levels.

Supporting Information Available: Tables of crystal data, structure solution and refinement, atomic coordinates, and bond distances and angles. This material is available free of charge via the Internet at http://pubs.acs.org.

IC000999R